Configurational temperature of multispecies dusty plasmas

Frank Wieben and Dietmar Block*
IEAP, Christian-Albrechts-Universität, D-24098 Kiel, Germany

Michael Himpel and André Melzer
Institute of Physics, University of Greifswald, 17489 Greifswald, Germany

(Received 31 May 2021; accepted 9 September 2021; published 14 October 2021)

The dust charge of the two species in a binary mixture of particles in a dusty plasma has been measured using the concept of configurational temperature. There, the dust charge and the respective dust charge ratio are determined from the comparison of the instantaneous particle positions and the kinetic temperature. For that purpose, experiments of binary mixtures of melamine-formaldehyde and silica particles have been evaluated. The configurational temperature approach has also been checked against simulations. From these analyses it is found that the charge ratio of the two species can be obtained quite accurately, whereas for the determination of the absolute charge values a good knowledge of the confining potential is required.

DOI: 10.1103/PhysRevE.104.045205

I. INTRODUCTION

Microscopic particles trapped in a plasma become charged by the electron and ion currents to the particle surface. For typical low temperature plasma conditions the particle attains a negative charge of about a few thousand elementary charges. These particles act as a third plasma component and significantly alter the plasma and its dynamics and give rise to structure formation.

For nearly all processes in dusty plasmas the particle charge is of central importance. However, to measure or calculate the particle charge is by far not trivial. Analytic models like the famous Orbital Motion Limit (OML) approach [1,2] make simplifying assumptions: the plasma is assumed to be isotropic, collisionless, and stationary, and an isolated dust grain is considered. In experiments, however, the particles are often confined and levitated in the plasma sheath above the lower electrode. There, the plasma generally is anisotropic and not quasineutral. Further, the ions are streaming with supersonic speed and the electrons are periodically leaving and entering the sheath region with each rf cycle. Hence, their distribution functions are usually quite complex. Often, also ion-neutral collisions play a role [3]. Finally, the dust grains are not isolated. They form a strongly coupled system where the interparticle distance is about the screening length [4–6]. Thus, a theoretical prediction of the charge of dust grains is still an open challenge.

Unfortunately, charge measurements are not trivial either. For example, the phase-resolved resonance method allows one to measure the charge-to-mass ratio with very high accuracy and can yield the absolute particle charge if the charge density in the sheath and the mass density of the particles are known [7], but it is limited to systems with a very few particles. For extended systems the charge can be measured via an analysis of the system dynamics. For small systems the normal modes analysis yields good results [8]. For large systems the dispersion relation of dust density waves can be utilized [9,10]. Recently, the dust charge of particles in a monodisperse, two-dimensional (2D) plasma crystal was measured from a comparison of the kinetic and so called configurational temperature [11,12]. The configurational temperature relies on the positions of the particles and not their dynamics, i.e., velocities. It was shown that this method allows one to measure the particle charge with good accuracy. Similarly, Mukherjee *et al.* [13] applied this technique to simulated and experimental data and compared configurational and kinetic temperatures.

The above mentioned approaches are generally designed for monodisperse systems, i.e., systems where all particles have the same size and thus the same charge. A charge measurement in a system with particles of different size is a difficult task. Tadsen *et al.* [14] showed that a local dispersion relation analysis can be used to determine the charge of monodisperse particles in an inhomogeneous plasma. From that, a local charge value could be derived. However, there the plasma (and thus charge) inhomogeneity is typically on a scale that is large compared to the interparticle distance.

In contrast, for binary or multispecies mixtures [15–24] one would be interested in the charge of the individual particles. In a binary mixture two species of particles with notably different charges form a mixed and strongly coupled system, where the local neighborhood of each particle contains particles of both species. So far only a heuristic comparison of interparticle distances in experiment and simulation allowed one to estimate a charge ratio of the two species. In a binary system of melamine-formaldehyde (MF) and silica (SiO_2) particles a charge ratio of $Q_{d,MF}/Q_{d,SiO_2} = 1.2 \pm 0.1$ was found [25]. Nevertheless, a true charge measurement for

*block@physik.uni-kiel.de

binary or multispecies mixtures of particles is still an open issue.

The configurational temperature method is a promising candidate for binary systems, as it directly exploits the individual particle positions and thus can take care of individual, local particle arrangements. A local, individual approach for binary or even multispecies complex plasmas would mark a significant step forward. On the one hand, it would allow one to directly obtain the charge ratio, which is a key parameter for binary mixtures with strong influence on structure and dynamics [26]. On the other hand, a measurement of the individual charges is desired for a comparison of local structures in experiments and simulations.

This paper presents methods which allow one to extend the configurational temperature approach, previously used in monodisperse systems [11,12], to binary mixtures. The technique will be benchmarked with simulation data and applied to experimental data. From that the charge ratio of the two species will be derived as well as the absolute particle charges.

II. THEORETICAL BACKGROUND

In a dusty plasma experiment, the full access to positions and velocities of all particles at all times directly allows one to determine the temperature from the velocity distribution function. For a Maxwellian velocity distribution the temperature can be obtained from the average kinetic energy per particle using $\frac{1}{2}m_\mathrm{d}\langle v^2\rangle = \frac{d}{2}k_\mathrm{B}T$ where d is the number of dimensions of the system, m_d is the particle mass, and v are the velocities. Here, the temperature T is defined via the dynamical properties of the particle ensemble.

A different approach has been suggested in 1997 by Butler *et al.* [27], based on prior work of Rugh [28]. This approach links the temperature to the fluctuations of the positions of the particles in a given potential and is summarized in the following.

For an arbitrary Hamiltonian system the temperature can be defined as

$$k_\mathrm{B}T = \frac{\langle \nabla \mathcal{H}(\mathbf{\Gamma}) \cdot \boldsymbol{B}(\mathbf{\Gamma})\rangle}{\langle \nabla \cdot \boldsymbol{B}(\mathbf{\Gamma})\rangle}. \tag{1}$$

Here, $\mathcal{H}(\mathbf{\Gamma}) = K(\{p_i\}) + U(\{q_i\})$ is the Hamiltonian of the system with the kinetic energy $K(\{p_i\})$ and the potential energy $U(\{q_i\})$. Further, $\mathbf{\Gamma} = \{q_1 ... q_{3N}, p_1 ... p_{3N}\}$ is the phase space of the system with the generalized coordinates q_i and generalized momentum p_i. $\boldsymbol{B}(\mathbf{\Gamma})$ can be any continuous and differentiable vector function in the phase space.

Choosing specifically $\boldsymbol{B}(\mathbf{\Gamma}) = -\nabla U(\{q_i\})$ yields a definition of temperature

$$k_\mathrm{B}T_\mathrm{conf} = \frac{\langle \nabla U(\{q_i\}) \cdot [-\nabla U(\{q_i\})]\rangle}{\langle -\nabla^2 U(\{q_i\})\rangle} = \frac{\langle \nabla U(\{q_i\}) \cdot \nabla U(\{q_i\})\rangle}{\langle \nabla^2 U(\{q_i\})\rangle}, \tag{2}$$

which is called configurational temperature [27,28]. According to Eq. (2), the configurational temperature depends on the generalized positions q_i only. The generalized momenta p_i and thus the dynamics of the system do not need to be known. Note that choosing $\boldsymbol{B}(\mathbf{\Gamma}) = (0, \dots 0, p_1, \dots p_N)$ yields the standard definition of the kinetic temperature.

For conservative forces, we can use $\boldsymbol{F} = -\nabla U$ to rewrite gradients in potential energy U as forces. For finite dusty plasmas basically two conservative forces are important: the restoring force of the confining trap $\boldsymbol{F}^\mathrm{c}$ and the electrostatic interaction forces between the particles $\boldsymbol{F}^\mathrm{int}$. Using $\boldsymbol{F} = \boldsymbol{F}^\mathrm{int} + \boldsymbol{F}^\mathrm{c}$ and Eq. (2) yields

$$k_\mathrm{B}T_\mathrm{conf} = \frac{\sum_{j=1}^{N}\left(\boldsymbol{F}_j^\mathrm{int} + \boldsymbol{F}_j^\mathrm{c}\right)^2}{-\left[\sum_{j=1}^{N}\nabla_j \cdot \left(\boldsymbol{F}_j^\mathrm{int} + \boldsymbol{F}_j^\mathrm{c}\right)\right]}. \tag{3}$$

Note that the sums indicate an average over the N particles in the system at a given instant. For a harmonic trap with $\boldsymbol{F}_j^c = -m_\mathrm{d}\omega_0^2\boldsymbol{q}_j = -k\boldsymbol{q}_j$ its divergence simply is $\nabla \cdot \boldsymbol{F}_j^c = -d\,k$ for particle j. Here, again d is the dimensionality and $k = m_\mathrm{d}\omega_0^2$ is the stiffness of the trap where ω_0 is the confinement frequency. Hence, for a 2D system in a harmonic confinement

$$k_\mathrm{B}T_\mathrm{conf} = \frac{\sum_{j=1}^{N}(\boldsymbol{F}_j^\mathrm{int} + \boldsymbol{F}_j^\mathrm{c})^2}{-\left[\sum_{j=1}^{N}\left(\nabla_j \cdot \boldsymbol{F}_j^\mathrm{int}\right) - 2Nk\right]}. \tag{4}$$

To calculate the configurational temperature the divergence of the interaction force is needed. For Yukawa interaction (i.e., a screened Coulomb interaction) this reads

$$\boldsymbol{F}_j^\mathrm{int} = \sum_{i\neq j}^{N}\frac{Q_{\mathrm{d},i}\,Q_{\mathrm{d},j}}{4\pi\epsilon_0}\left(\frac{1}{r_{ij}^2} + \frac{1}{r_{ij}\lambda_\mathrm{s}}\right)\exp\left(-\frac{r_{ij}}{\lambda_\mathrm{s}}\right)\boldsymbol{e}_{ij}, \tag{5}$$

with $r_{ij} = \sqrt{(x_i - x_j)^2 + (y_i - y_j)^2}$ as the distance between a particle pair and $\boldsymbol{e}_{ij}$ as the unit vector in direction of the force. The divergence of the interaction force then is

$$\nabla_j \cdot \boldsymbol{F}_j^\mathrm{int} = \frac{\partial F_{j,x}^\mathrm{int}}{\partial x_j} + \frac{\partial F_{j,y}^\mathrm{int}}{\partial y_j}. \tag{6}$$

For the x direction

$$\frac{\partial F_{j,x}^\mathrm{int}}{\partial x_j} = \sum_{i\neq j}^{N}\frac{Q_{\mathrm{d},i}\,Q_{\mathrm{d},j}}{4\pi\epsilon_0}\exp\left(-\frac{r_{ij}}{\lambda_\mathrm{s}}\right)\left[\frac{3\Delta x^2}{r_{ij}^5} + \frac{3\Delta x^2}{r_{ij}^4\lambda_\mathrm{s}} + \frac{\Delta x^2}{r_{ij}^3\lambda_\mathrm{s}^2} - \frac{1}{r_{ij}^3} - \frac{1}{r_{ij}^2\lambda_\mathrm{s}}\right], \tag{7}$$

with $\Delta x = x_i - x_j$. The other directions are calculated alike.

The full divergence $\nabla_j \cdot \boldsymbol{F}_j^{\rm int}$ using $\Delta x^2 + \Delta y^2 = r_{ij}^2$ yields

$$\nabla_j \cdot \boldsymbol{F}_j^{\rm int} = \frac{\partial F_{j,x}^{\rm int}}{\partial x_j} + \frac{\partial F_{j,y}^{\rm int}}{\partial y_j} = \sum_{i\neq j}^{N} \frac{Q_{{\rm d},i}\, Q_{{\rm d},j}}{4\pi\epsilon_0} \exp\left(-\frac{r_{ij}}{\lambda_{\rm s}}\right)\left[\frac{1}{r_{ij}^3} + \frac{1}{r_{ij}^2\lambda_{\rm s}} + \frac{1}{r_{ij}\lambda_{\rm s}^2}\right]. \tag{8}$$

With Eqs. (3) and (8) we can now determine the configurational temperature of the system from its positions if the particle charge $Q_{\rm d}$, screening length $\lambda_{\rm s}$, and confinement (e.g., in terms of the trap stiffness k) are given. Note that for a binary system the particle charge of the two species is different and that thus the individual charges $Q_{{\rm d},i}$ and $Q_{{\rm d},j}$ might differ.

One can regard the configurational temperature as a measure of to what extent deviations from the force balance on the particles, described by the numerator of the right-hand side of Eq. (3), lead to particle displacements in the effective confining potential of external confinement and particle interaction around equilibrium, as given by the denominator. This gives us a handle on how to extract the dust charges from the configurational temperature.

First, we exploit that the system is, on average, in force equilibrium, i.e.,

$$\left\langle \sum_{j=1}^{N} \boldsymbol{F}_j^{\rm int} + \boldsymbol{F}_j^{\rm c} \right\rangle_t = \boldsymbol{0}, \tag{9}$$

where $\langle\cdot\rangle_t$ denotes the temporal average.

Second, on the basis of the equipartition theorem, we can assume that the configurational temperature is a measure of the dynamical state of the system and, hence, should match the kinetic temperature of the system, i.e., $T_{\rm kin} = T_{\rm conf}$. Using the kinetic temperature information in dusty plasmas from the particle velocities v_j and the relation

$$\begin{aligned} k_{\rm B}T_{\rm kin} &= \frac{1}{Nd} m_{\rm d} \left\langle \sum_{j=1}^{N} v_j^2 \right\rangle_t \\ &= k_{\rm B}T_{\rm conf} = \frac{\sum_{j=1}^{N} \left(\boldsymbol{F}_j^{\rm int} + \boldsymbol{F}_j^{\rm c}\right)^2}{-\left[\sum_{j=1}^{N} \nabla_j \cdot \left(\boldsymbol{F}_j^{\rm int} + \boldsymbol{F}_j^{\rm c}\right)\right]}, \end{aligned} \tag{10}$$

it is possible to determine particle charge $Q_{\rm d}$ (or particle charges of the two species in a binary mixture) from the particle positions. The (unknown) screening length $\lambda_{\rm s}$ and the trap confinement are determined with an iterative approach as described below.

Finally, it is clear that this method relies on the correct description of the interaction and confinement forces. In principle, any conservative force mixture can be used to compute Eq. (2). In our situation, the interaction between dust particles in a two-dimensional dust cluster can be very well described by a screened Coulomb (Yukawa) interaction [9,29–31], as it is done here and in the previous analysis of monodisperse systems [11]. In extended systems in the plasma sheath where wake field effects [32–34] might play a role probably more sophisticated force models have to be derived and applied.

III. CHARGE ESTIMATION FROM SIMULATION DATA

A. Monodisperse systems

This section will introduce the scheme that can be used to determine the dust charge using simulation data. We start here with a simple monodisperse 2D dust system in a harmonic confinement. This will then be extended to binary mixtures.

Our simulation code is a standard Langevin dynamics simulation approach. Although we are preferably interested in 2D systems the code handles positions and velocities in three dimensions. In the radial (horizontal) direction the particles are confined in a harmonic trap of stiffness $k_{\rm sim} = 2.2 \times 10^{-11}\,{\rm kg\,s^{-2}}$. The third (vertical) dimension has a stronger confinement to force the system into a single layer. However, this vertical confinement is finite to address the levitation condition in a binary mixture correctly. Either monodisperse particles or binary mixtures of particles are treated in the simulation. For binary systems, our simulation reproduces the mixing and demixing of binary systems. Mixed systems are observed only if the charge-to-mass ratios of both particle species are equal, i.e., a charge disparity of the two species also requires a mass disparity. For the simulations all parameters are in absolute values and are chosen similar to the experimental conditions. More details about the simulation are found in [25,35].

We now start with the analysis of a monodisperse system: By definition, all forces on the particles balance on average in equilibrium, hence $\langle \boldsymbol{F}^{\rm c} + \boldsymbol{F}^{\rm int}\rangle_t = 0$. Further, if charge $Q_{\rm d}$ and screening length $\lambda_{\rm s}$ are known, the interaction force $\boldsymbol{F}^{\rm int}$ can be calculated and, from that, the confinement force $\boldsymbol{F}^{\rm c} = -\boldsymbol{F}^{\rm int}$ can be estimated. Hence, for any meaningful set of parameters $\{Q_{\rm d}, \lambda_{\rm s}\}$ we first calculate the interparticle forces $\boldsymbol{F}^{\rm int}$ from the particle positions. Figure 1(a) shows the calculated x component of $\boldsymbol{F}^{\rm int}$ as a function of the x coordinate of the particles for an arbitrary choice of $\{Q_{\rm d}, \lambda_{\rm s}\}$. This interaction force has to be balanced by the trap force to obtain equilibrium. In a harmonic trap the trapping force scales linearly with x and the stiffness of the trap simply is the slope $k = m_{\rm d}\omega_0^2$. This procedure yields an individual trap stiffness for each set of $\{Q_{\rm d}, \lambda_{\rm s}\}$. If $\{Q_{\rm d}, \lambda_{\rm s}\}$ are chosen as in the simulation, the confinement force reconstructed from the interaction force exactly matches the trap stiffness $k_{\rm sim} = 2.2 \times 10^{-11}\,{\rm kg\,s^{-2}}$ used in the simulation. This is a nice consistency check, but it should be noted that this first step does not allow one to determine which is the correct set of $\{Q_{\rm d}, \lambda_{\rm s}\}$, yet.

Next, for each pair of $\{Q_{\rm d}, \lambda_{\rm s}\}$ together with the fitted trap stiffness k from the force balance we determine the configurational temperature from Eq. (3). This configurational temperature then is compared with the kinetic temperature $(Nd/2)k_{\rm B}T_{\rm kin} = (1/2)m_{\rm d}\langle v^2\rangle$.

To illustrate the method, the residual

$$R(Q_{\rm d}, \lambda_{\rm s}) = |T_{\rm kin} - T_{\rm conf}(Q_{\rm d}, \lambda_{\rm s}, k)| \tag{11}$$

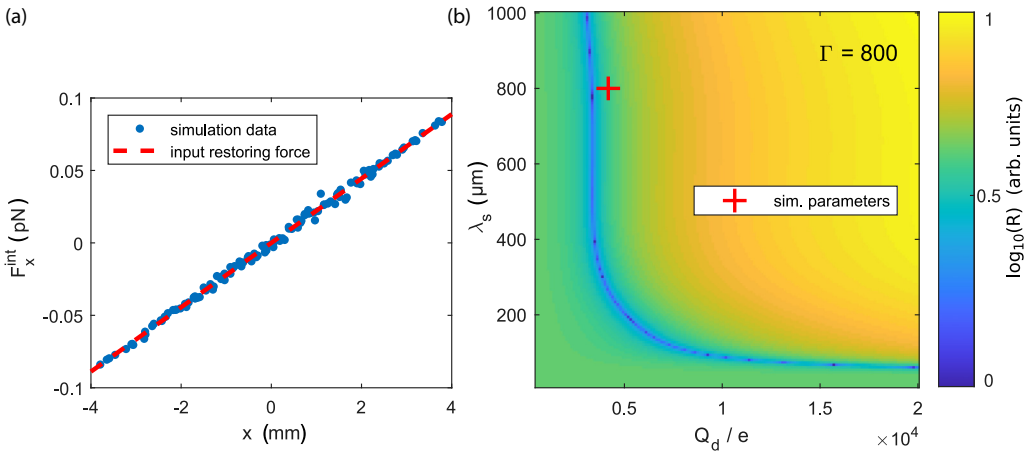

FIG. 1. (a) Interparticle force as a function of the particles' x coordinate. The confinement is harmonic with a slope $k_x = m\omega_0^2$. The red dashed line indicates the confinement force used in the simulation. (b) Map (color-coded) of the residuals R between configurational and kinetic temperature in the $\{Q_d, \lambda_s\}$ plane for a case with moderate coupling ($\Gamma = 800$). Γ values were determined according to the model of Vaulina *et al.* [36]. The region $\lambda_s(Q_d)$ of lowest residual indicates where configurational and kinetic temperature are equal. The red cross denotes the parameters used in the simulations.

is calculated for each parameter pair $\{Q_d, \lambda_s\}$ (and fitted k). An example of such a residual map is shown in Fig. 1(b), where we used just the particle positions $\{x_1 \ldots x_N, y_1 \ldots y_N\}$ from a single time step of the simulation to calculate the configurational temperature. Generally, any pair of Q_d and λ_s with a vanishing residual of R is a possible solution (blue line).

In the calculation of the configurational temperatures the interactions between all particles are taken into account. For a given particle, the total force is zero in equilibrium. Hence, for this particle, the contribution to the configurational temperature is mainly determined from the configurational deviations from equilibrium positions with respect to its nearest neighbors since there the relative displacements to the given particle are largest. Moreover, the influence of distant particles is reduced by the exponential factor in the Yukawa interaction. As a consequence, the reconstructed particle charge is nearly independent of the screening length λ_s. Only when λ_s becomes decisively smaller than the interparticle distance, e.g., when $\lambda_s < 250\,\mu$m for our parameters, the electrostatic forces between particles are effectively screened by the plasma and the stronger screening has to be compensated by increased charges on the particles [see Fig. 1(b)]. Since in typical dusty plasma experiments the screening length is of the order of the interparticle distance, i.e., of the order of a few hundred microns [9,29,30], the chosen screening length fortunately has only little influence on the derived charge.

B. Binary systems

We now extend these findings to binary systems which will introduce two main changes in the algorithm. First, we have to account for the fact that now two independent coefficients $k_i = m_{d,i}\omega_0^2$ for the confinement of two particle species are necessary as they have different masses. In Fig. 2 we show the x component of the confinement force against the x position of the particle for each of the two species. In our simulation data, the linear dependence of the force with x is very good. The linear model nicely fits the data. Further, we can calculate the deviation between the interparticle forces and the confinement force with the fitted coefficients k_i. Figure 3 nicely shows on a $Q_{d,1}/Q_{d,2}$ grid that the minimum residual for the force balance is well fitted by a linear relation (dashed line). Thus, the best force balance is achieved for fixed charge ratio Q_{d1}/Q_{d2}.

As a second modification, a measure for the total kinetic temperature of a binary mixture has to be defined, because the kinetic temperatures of each species obtained from the velocity distributions, $T_{kin,1}$ and $T_{kin,2}$, are slightly different. Hence, since in the simulation we have an equal amount of particles of each species, we can take the average of $T_{kin,1}$ and $T_{kin,2}$ as a measure for the temperature of the binary mixture, i.e., $T_{bin} = (T_{kin,1} + T_{kin,2})/2$.

With these values of k_i and T_{bin} it is now possible to compute residual maps of configurational and kinetic temperatures. These maps generally depend on three quantities now, Q_{d1}, Q_{d2}, and λ_s. Guided by the finding from monodisperse systems, where the choice of λ_s had only little influence on the result and the fact that this influence should be identical for Q_{d1} and Q_{d2}, we chose λ_s being equal to the interparticle

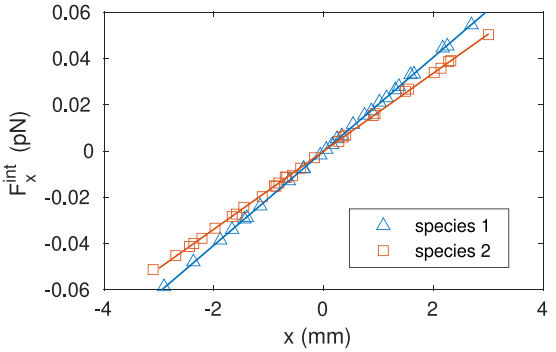

FIG. 2. The interparticle force on the particles for the two simulated species in the binary mixture. The simulated linear confinement force can be retrieved by the linear fits.

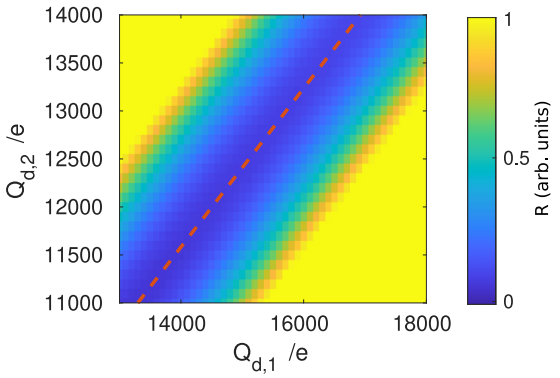

FIG. 3. Map (color-coded) of the deviation between interparticle forces and the confinement force with the fitted coefficients k_i. The region of smallest residuals forms a straight line (dashed line) in the $\{Q_{d1}, Q_{d2}\}$ plane.

distance. A typical result of such a residual map is shown in Fig. 4.

Here, the region of smallest residuals is indicated by the solid curve and is well described by a rotated parabola in the $\{Q_{d1}, Q_{d2}\}$ space. Hence, there are in general two pairs of $\{Q_{d1}, Q_{d2}\}$ that yield equal kinetic and configurational temperatures, except for the cusp of the parabola. Interestingly, this is nearly exactly where the simulation input parameters are found. In addition, this is also the point on the curve that coincides with the force balance condition $\langle \boldsymbol{F}^{c} + \boldsymbol{F}^{int} \rangle_t = 0$ (dashed line).

Having this intersection of the force-balance line and the parabolalike curve in Fig. 4, the cusp of the parabola on its own already seems to be sufficient information to extract the charge ratio and the absolute charge of the two particle species. The cusp of the parabola shown in Fig. 4 yields the absolute charges of species 1 and 2 as $Q_{d,1} = 15\,725\,e$ and $Q_{d,2} = 13\,000\,e$, which agree well with the simulation values of $Q_{d,1} = 15\,855\,e$ and $Q_{d,2} = 13\,169\,e$. We did also ensure that the cusp is a valid guess for a larger range of charge ratios. From numerous other simulations (see Fig. 5), it is

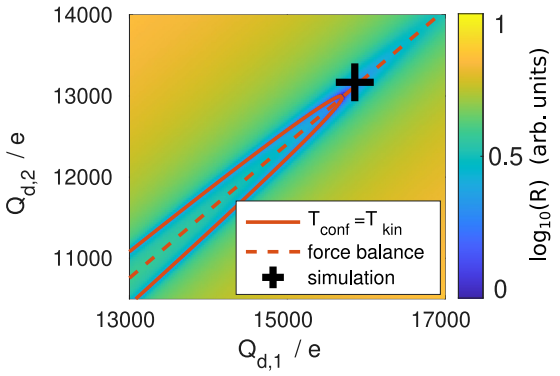

FIG. 4. Map (color-coded) of the residuals between configurational and kinetic temperature computed according to Eq. (10). The region of smallest residuals forms a rotated parabola (solid line) in the $\{Q_{d1}, Q_{d2}\}$ plane. The charges used in the simulation are found near the cusp of the parabola (cross). The dashed line indicates the force balance from Fig. 3.

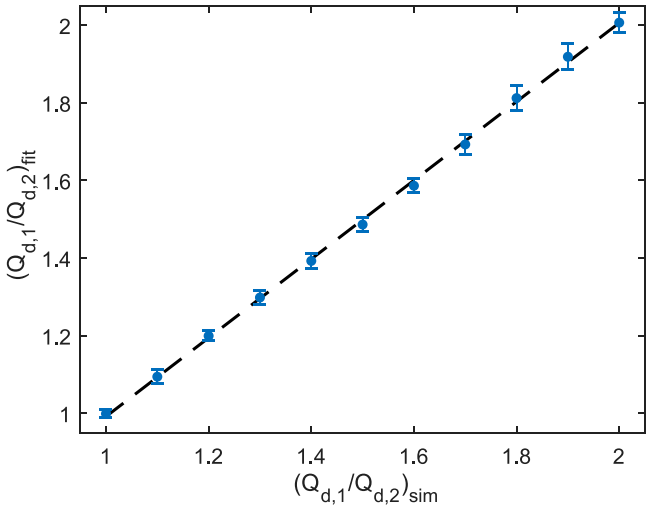

FIG. 5. The determined charge ratios $(Q_{d,1}/Q_{d,2})_{fit}$ for different simulation parameters of $(Q_{d,1}/Q_{d,2})_{sim}$. The data points are the average values for several simulation time steps. The errorbars indicate the standard deviation.

learned that the cusp of the parabola always yields a very good estimate for the charge ratio of $Q_{d,1}$ and $Q_{d,2}$.

Note that the absolute charge values somewhat deviate from the expected particle charge. These deviations are caused by our rough estimation of the screening length. However, this error is the same for both species. As λ_s is the effective screening length provided by the plasma electrons and ions it should be identical for both particle species and thus cancels out in the charge ratio. Further, it has to be noted that our method already works with a single set of particle positions. Except for Fig. 5 no averaging was used.

IV. CHARGE ESTIMATION FROM EXPERIMENTAL DATA

Now, we apply the above method to experimental data. The measurements were performed at the LAMA experiment in Kiel [25]. It is a capacitively coupled asymmetric discharge which is typically operated at low rf power ($P_{rf} \approx 12$W) and low neutral gas pressure ($p_{Ar} \approx 6$Pa). In this experiment we use SiO_2 and MF particles. While the SiO_2 species is stable the MF-particle radius changes due to etching by the plasma components. The etching rate is $\Delta a_{MF}/\Delta t \approx -1.25\,\mathrm{nm/min}$ [37]. Thus, the particle charge of the SiO_2 species is constant and the charge and mass of the MF species decrease as a function of time. As charge and mass loss depend differently on particle radius the charge-to-mass ratio of the MF species changes. This results in a changing levitation height. At the point of equal levitation height of the two species their charge-to-mass ratio matches and this way we can create a binary mixture.

The experiment is started with MF particles of $a_{MF} = 4.43\,\mu$m radius and SiO_2 particles of $s_{SiO_2} = 3.69\,\mu$m radius that are dropped into the discharge and that then, due to their different masses, settle at different heights in the plasma sheath. Now, by plasma etching, the MF-particle size reduces with time until equal levitation heights are reached. From the etch rate and the time until an equal levitation height is

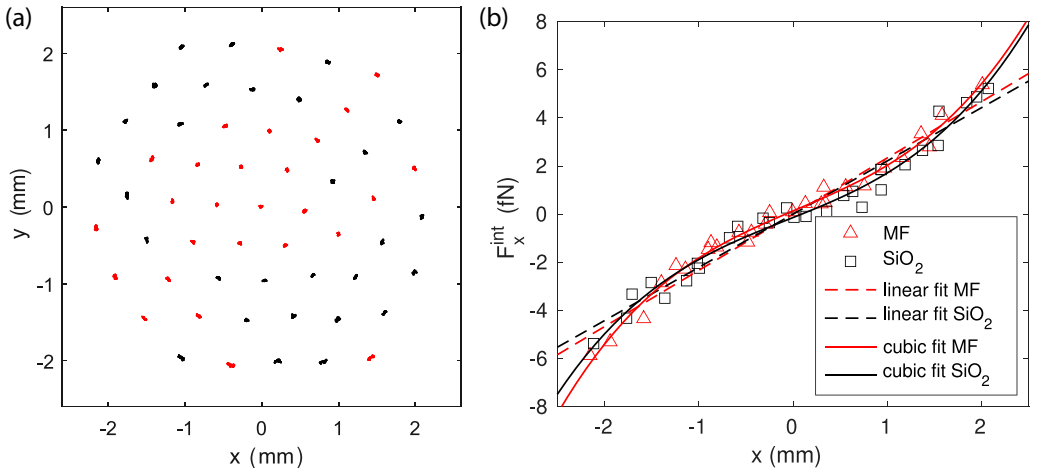

FIG. 6. (a) Trajectories of a strongly coupled binary system consisting of MF (red) and SiO_2 particles (black). The image shows a time interval of $t = 2.8$ s. (b) The x component of the interparticle force for both particle species (red triangles and black squares). The linear (dashed line) and the cubic (solid line) fit for a matching confinement force are shown for each species.

reached the MF-particle size can be estimated to be $a_{\mathrm{MF}} = 4.25 \pm 0.06\,\mu\mathrm{m}$ when both particle species form a binary mixture.

The measured particle trajectories in 500 consecutive frames (the frame rate was 180 fps) are shown in Fig. 6(a). The binary mixture consists of 56 particles (27 MF and 29 SiO_2 particles) and shows particles of both species evenly distributed in radial and poloidal position. The system is obviously in a strongly coupled state and only thermal motion around the equilibrium position is observed.

We will now perform the charge analysis for our experimental system. First, the kinetic temperature was measured for the two different species. Here, from the experimental data of the particle velocities we derive $T_{\mathrm{kin,MF}} = 637$ K and $T_{\mathrm{kin,SiO_2}} = 445$ K for the two species resulting in the mean (weighted with particle number) temperature $T_{\mathrm{kin}} = 538$ K. The configurational temperature now accounts for the energy stored in the particle-particle interactions and the confinement. From equipartition these two temperatures are taken equal [see Eq. (10)].

Hence, as the next step it is necessary to determine the confinement force. In Fig. 6(b), we present the confinement force alongside with a linear (dashed lines) and a cubic (solid lines) fit of the data. Especially in the outer regions of the cluster, it is obvious that a linear model results in large deviations of the data points from the fitted curve. That would result in larger configurational temperatures and finally in lower charges that will be determined. We will thus use the cubic force model (corresponding to a confining potential that is proportional to x^4) in the following, i.e.,

$$F_x^{\mathrm{c}} = -(k_1 x^3 + k_2 x^2 + k_3 x + k_4). \tag{12}$$

Then, we compute the residual map between configurational and kinetic temperature in a parameter regime of $\{Q_{\mathrm{d,MF}}, Q_{\mathrm{d,SiO_2}}\}$ (the screening length was first taken as $\lambda_{\mathrm{s}} = 500\,\mu\mathrm{m}$, here). The resulting map and the corresponding force balance condition line are shown in Fig. 7. The force balance $\langle \boldsymbol{F}^{\mathrm{c}} + \boldsymbol{F}^{\mathrm{int}} \rangle = 0$ was determined as shown above using a cubic confinement force model over the particle ensemble. In Fig. 7 one finds, like in the simulation case, the region of smallest residuals that forms a rotated parabola in the $\{Q_{\mathrm{d,MF}}, Q_{\mathrm{d,SiO_2}}\}$ parameter space. And again the force balance condition intersects the parabola at the cusp. For completeness, here we also added the parabolic curves that are obtained using different screening lengths $\lambda = 300$ and $700\,\mu\mathrm{m}$. The resulting charges differ with screening length, but for the two larger screening lengths ($\lambda = 500$ and $700\,\mu\mathrm{m}$) the difference is quite small, as discussed above. Please also note that the charge ratio is unaffected by the choice of λ, as all of the three force balance lines are nearly indistinguishable. From the intersection of the force balance with the equality of the two temperatures we derive $Q_{\mathrm{d,MF}} = 2500\,e$ and $Q_{\mathrm{d,SiO_2}} = 2220\,e$ (using $\lambda = 500\,\mu\mathrm{m}$).

In principle, the above analysis can be performed for each frame individually since it requires only the particle positions. Hence, the fluctuations of the measured charge ratio could be analyzed to benchmark the stability and reproducibility of the method. Therefore, we analyzed a sequence of 1000 images. For intervals of 20 frames length the kinetic temperature was measured and compared to the configurational temperature. In combination with the force balance, for each interval the charge ratio was determined. The results are shown in Fig. 8. For our binary mixture we find a charge ratio $Q_{\mathrm{d,MF}}/Q_{\mathrm{d,SiO_2}} =$

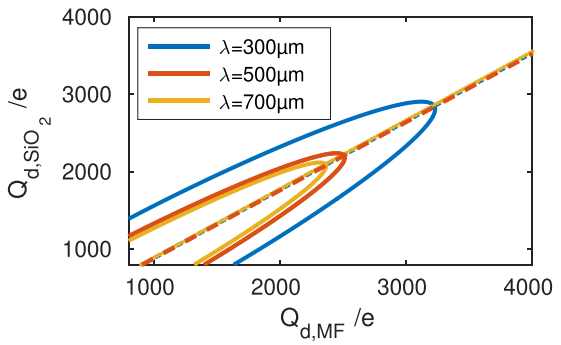

FIG. 7. The solid lines indicate the region where configurational and kinetic temperature coincide (solid lines) in the $\{Q_{\mathrm{d,MF}}, Q_{\mathrm{d,SiO_2}}\}$ plane for different values of the assumed screening length λ_{s}. The dashed lines indicate the respective force balance.

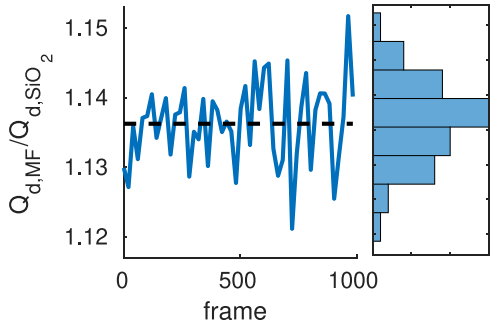

FIG. 8. Charge ratios obtained from the experimental measurement. From a sequence of 1000 frames length, for each interval of 20 frames length, the charge ratio has been evaluated. The right panel indicates the derived histogram of the charge ratios.

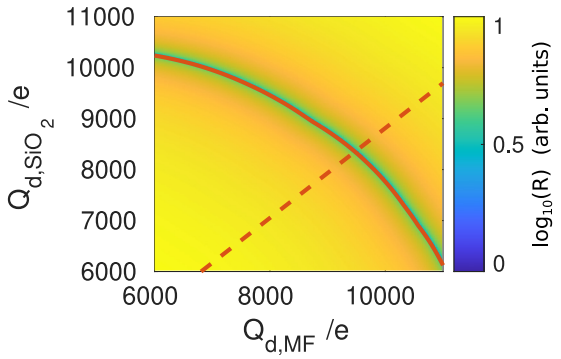

FIG. 9. Map (color-coded) of the residuals between configurational and kinetic temperature in the $\{Q_{d,MF}, Q_{d,SiO_2}\}$ plane using individual confinements. The dashed force balance line is the force balance condition from Fig. 7.

1.137 ± 0.01 (for the fixed chosen screening length λ_s). Accounting for the uncertainty in the screening length one finds $Q_{d,MF}/Q_{d,SiO_2} = 1.14 \pm 0.02$, which matches the previously reported value of $Q_{d,MF}/Q_{d,SiO_2} = 1.2 \pm 0.1$ [25] very well. In addition, the fluctuations for the charge ratio are very small. Thus we conclude that the used method yields stable and precise values for experimental as it did for simulation data. It is also interesting to note that the particle sizes in the binary mixture behave very similarly as the dust charges, namely, as $a_{MF}/a_{SiO_2} = 1.15 \pm 0.02$. This indicates that the dust charges scale directly proportional to the dust size as expected from an OML model.

While the so determined charge ratio is reasonable the absolute values of the dust charges seem quite low. The main reason of this low charge can be found in the model of the confinement force. The better our chosen model of $\boldsymbol{F}^c$ fits the behavior of $\boldsymbol{F}^{int}$ the smaller is the numerator in the determination of the configurational temperature in Eq. (3) and, consequently, the configurational temperature itself. Thus, higher dust charges are required to match the kinetic temperature. It should be noted that even for the chosen cubic model there are notable deviations from the force balance for individual particles, since the model is an approximation over all particles of the species. In the denominator of Eq. (3), the influence of the chosen model for the local confinement strength is minor. The denominator is mainly determined by the divergence of the interaction force.

Above, the confinement force $\boldsymbol{F}^c$ was approximated by a cubic relation that was fitted to the spatial behavior over the ensemble of MF and SiO_2 particles, respectively. As mentioned above, on the one hand, this procedure could be done for each frame since the method only requires the instantaneous particle positions $\{x_1 \ldots x_N, y_1 \ldots y_N\}$. On the other hand, the force balance $\langle \boldsymbol{F}^{int} \rangle = -\langle \boldsymbol{F}^c \rangle$ should be fulfilled as precisely as possible. For simulation data, where the confinement potential is accurately known these two conditions can be fulfilled easily. In experiments, the confinement is generally not known that precisely.

A possible solution is to take into account temporally averaged particle positions $\{\langle x_1 \rangle_t \ldots \langle x_N \rangle_t, \langle y_1 \rangle_t \ldots \langle y_N \rangle_t\}$ where the temporal average is taken over the frames of interest. Then, we assign an individual trap stiffness k_j to each of the particles j by simply setting $F^c_{jx} = -k_j \langle x_j \rangle_t$ (and equivalently for the y component). The difference to the above situation is that we have an individual trap stiffness k_j for each of the particles instead of a global k for the entire system (or species).

In doing so, the force balance $\langle \boldsymbol{F}^{int}_j \rangle = -\langle \boldsymbol{F}^c_j \rangle$ is fulfilled exactly for each particle (as a temporal average) and now only the positional fluctuations around this individual equilibrium play a role for calculating the configurational temperature. This again reduces the numerator in the determination of the configurational temperature in Eq. (3) and, consequently, the configurational temperature itself, leading to higher particle charges. The result of this approach using the individual trap stiffness k_j is shown in Fig. 9.

It can be seen that the resulting residual map in the $\{Q_{d,MF}, Q_{d,SiO_2}\}$ space still features a curved region of smallest residuals, shifted to even higher charge values. As we do not model a global confinement now, there is no possibility to use the deviations from it to exploit the force balance condition. Thus, to find the right point to extract the particle charges in the graph in Fig. 9, we use the force balance condition from Fig. 7 again. By keeping the information that the charge ratio is reliably determined to be around 1.14 we derive $Q_{d,MF} = 9400\,e$ and $Q_{d,SiO_2} = 8285\,e$. These absolute charge values seem much more realistic than the previous, indicating that it is really necessary to fulfill the force balance as precisely as possible.

In the combination of the results, we can conclude that the discussed approach using the configurational temperature is able to reliably determine the charge ratio as 1.14, in this case. The absolute values of the dust charges are found in an expected range if the force balance is fulfilled (in a temporal average) for each particle individually. The dependence on the screening length is not very strong.

V. SUMMARY

The configurational temperature has previously been used for the analysis of monodisperse systems and has now been extended to binary dusty plasmas. The configurational temperature makes use of the particle positions alone. In addition, also the force balance has to be utilized. In a first step, this approach has been tested against simulations.

In a second step, using experimental data, the configurational temperature has been determined in a binary dust system. From the comparison of the configurational temperature with the kinetic temperature the dust charge ratio of the two species has been derived with very high accuracy as $Q_{d,MF}/Q_{d,SiO_2} = 1.14 \pm 0.02$ in agreement with previous estimations [25] and the dust size ratio indicating a direct proportionality between dust charge and size as expected from OML.

Further, it has been demonstrated that for a reliable determination of absolute charges of the two species the confinement potential has to be modeled as closely as possible. Best results were obtained by fulfilling the force balance exactly (as a temporal average) and use only the deviations from this temporally averaged equilibrium to determine the configurational temperatures.

ACKNOWLEDGMENTS

Financial support by the German Aerospace Center under Contract No. 50 WM 1962 and Deutsche Forschungsgemeinschaft under Grants No. Me1534/8-1 and No. Bl555/3-1 is gratefully acknowledged.

[1] H. M. Mott-Smith and I. Langmuir, Phys. Rev. **28**, 727 (1926).
[2] T. Nitter, Phys. Scr. **5**, 93 (1996).
[3] S. A. Khrapak, S. V. Ratynskaia, A. V. Zobnin, A. D. Usachev, V. V. Yaroshenko, M. H. Thoma, M. Kretschmer, H. Höfner, G. E. Morfill, O. F. Petrov, and V. E. Fortov, Phys. Rev. E **72**, 016406 (2005).
[4] *Dusty Plasmas*, edited by A. Bouchoule (Wiley, New York, 1999).
[5] P. K. Shukla and A. A. Mamun, *Introduction to Dusty Plasma Physics* (Institute of Physics, University of Reading, Berkshire, 2002).
[6] A. Melzer, *Physics of Dusty Plasmas: An Introduction* (Springer, New York, 2019).
[7] O. H. Asnaz, H. Jung, F. Greiner, and A. Piel, Phys. Plasmas **24**, 083701 (2017).
[8] A. Melzer, Phys. Rev. E **67**, 016411 (2003).
[9] S. Nunomura, J. Goree, S. Hu, X. Wang, and A. Bhattacharjee, Phys. Rev. E **65**, 066402 (2002).
[10] B. Tadsen, F. Greiner, and A. Piel, Phys. Plasmas **21**, 103704 (2014).
[11] M. Himpel and A. Melzer, Phys. Rev. E **99**, 063203 (2019).
[12] M. Himpel and A. Melzer, Phys. Rev. E **101**, 029902(E) (2020).
[13] R. Mukherjee, S. Jaiswal, M. K. Shukla, A. Hakim, and E. Thomas, Contrib. Plasma Phys. **60**, e201900161 (2020).
[14] B. Tadsen, F. Greiner, and A. Piel, Phys. Plasmas **24**, 033704 (2017).
[15] M. Mikikian, L. Boufendi, A. Bouchoule, H. M. Thomas, G. E. Morfill, A. P. Nefedov, V. E. Fortov, and the PKE-Nefedov team, New J. Phys. **5**, 19 (2003).
[16] G. E. Morfill, U. Konopka, M. Kretschmer, M. Rubin-Zuzic, H. M. Thomas, S. K. Zhdanov, and V. Tsytovich, New J. Phys. **8**, 06221 (2006).
[17] K. R. Sütterlin, A. Wysocki, A. V. Ivlev, C. Räth, H. M. Thomas, M. Rubin-Zuzic, W. J. Goedheer, V. E. Fortov, A. M. Lipaev, V. I. Molotkov, O. F. Petrov, G. E. Morfill, and H. Löwen, Phys. Rev. Lett. **102**, 085003 (2009).
[18] K. Jiang, L.-J. Hou, A. V. Ivlev, Y.-F. Li, C.-R. Du, H. M. Thomas, G. E. Morfill, and K. R. Sütterlin, Europhys. Lett. **93**, 55001 (2011).
[19] C.-R. Du, K. R. Sütterlin, K. Jiang, C. Räth, A. V. Ivlev, S. Khrapak, M. Schwabe, H. M. Thomas, V. E. Fortov, A. M. Lipaev, V. I. Molotkov, O. F. Petrov, Y. Malentschenko, F. Yurtschichin, Y. Lonchakov, and G. E. Morfill, New J. Phys. **1**, 073058 (2012).
[20] A. Wysocki, C. Räth, A. V. Ivlev, K. R. Sütterlin, H. M. Thomas, S. Khrapak, S. Zhdanov, V. E. Fortov, A. M. Lipaev, V. I. Molotkov, O. F. Petrov, H. Löwen, and G. E. Morfill, Phys. Rev. Lett. **105**, 045001 (2010).
[21] M. Schwabe and D. B. Graves, Phys. Rev. E **88**, 023101 (2013).
[22] C. Killer, T. Bockwoldt, S. Schütt, M. Himpel, A. Melzer, and A. Piel, Phys. Rev. Lett. **116**, 115002 (2016).
[23] S. Schütt, M. Himpel, and A. Melzer, Phys. Rev. E **101**, 043213 (2020).
[24] S. Schütt and A. Melzer, Phys. Rev. E **103**, 053203 (2021).
[25] F. Wieben, J. Schablinski, and D. Block, Phys. Plasmas **24**, 033707 (2017).
[26] G. J. Kalman, P. Hartmann, Z. Donkó, K. I. Golden, and S. Kyrkos, Phys. Rev. E **87**, 043103 (2013).
[27] B. D. Butler, G. Ayton, O. G. Jepps, and D. J. Evans, J. Chem. Phys. **109**, 6519 (1998).
[28] H. H. Rugh, Phys. Rev. Lett. **78**, 772 (1997).
[29] U. Konopka, G. E. Morfill, and L. Ratke, Phys. Rev. Lett. **84**, 891 (2000).
[30] A. Homann, A. Melzer, S. Peters, and A. Piel, Phys. Rev. E **56**, 7138 (1997).
[31] J. Carstensen, F. Greiner, and A. Piel, Phys. Plasmas **17**, 083703 (2010).
[32] S. V. Vladimirov and M. Nambu, Phys. Rev. E **52**, R2172 (1995).
[33] M. Nambu, S. V. Vladimirov, and P. K. Shukla, Phys. Lett. A **203**, 40 (1995).
[34] V. A. Schweigert, I. V. Schweigert, A. Melzer, A. Homann, and A. Piel, Phys. Rev. E **54**, 4155 (1996).
[35] F. Wieben, Struktur und Dynamik binärer komplexer Plasmen, Ph.D. thesis, Christian-Albrechts-Universität Kiel, 2021.
[36] O. Vaulina, S. Khrapak, and G. Morfill, Phys. Rev. E **66**, 016404 (2002).
[37] N. Kohlmann, F. Wieben, O. H. Asnaz, D. Block, and F. Greiner, Phys. Plasmas **26**, 053701 (2019).